Diverging elasticity and director uniformation in a nanopatterned cell near the nematic–smectic-*A* phase transition

Timothy J. Atherton, Ruiting Wang, and Charles Rosenblatt
Department of Physics, Case Western Reserve University, Cleveland, Ohio 44106-7079, USA
(Received 30 January 2008; published 2 June 2008)

The stylus of an atomic force microscope is used to scribe herringbone patterns of various wavelengths into a polyimide-coated substrate. The patterns serve as a template for alignment of the liquid crystal octyloxycyanobiphenyl and impose a bend distortion in the liquid crystal in the vicinity of the herringbone apexes. The pretransitional behavior of the liquid crystal is observed by polarized microscopy as it is cooled through the nematic–smectic-*A* phase transition, facilitating direct visualization of the extrapolation length, which is related to the trade-off between elastic and anchoring forces. Just above the phase transition temperature the expulsion of bend deformation is observed and is shown to be in good quantitative agreement with continuum theory. Very close to the transition temperature a weak threshold behavior is observed, wherein the smectic-*A* phase forms a monodomain for short period herringbones, but breaks into multiple domains when the patterned period is large.

DOI: 10.1103/PhysRevE.77.061702 PACS number(s): 61.30.Hn, 61.30.Jf

I. INTRODUCTION

The transition from the nematic phase to the smectic-*A* phase in liquid crystals is one of the classic problems of condensed matter physics [1–3]. Characteristic of the transition are two geometric constraints imposed by the smectic order: The layers must be continuous throughout the material, and because the layers are nearly incompressible, they must be spaced equally. The latter constraint serves to forbid twist and bend deformations of the director $\hat{n}$, i.e., those that depend on the curl of the director field, from the bulk smectic in a manner analogous to the Meissner effect in a type-I superconductor [1,4]. Above the transition temperature T_{NA} one finds bulk smectic fluctuations that are characterized by correlation lengths $\xi_{\parallel}$ and $\xi_{\perp}$ parallel and perpendicular to $\hat{n}$, respectively, that diverge as $T \rightarrow T_{NA}$. These fluctuations have the effect of expelling the forbidden twist and bend deformations from the bulk nematic. The corresponding elastic constants K_{22} and K_{33}, whose critical parts scale as $\xi_{\perp}^2/\xi_{\parallel}$ and $\xi_{\parallel}$, respectively, therefore diverge on cooling toward T_{NA} [1].

Recently our group demonstrated that a short wavelength bulk bend deformation may be imposed on a nematic liquid crystal by patterning a polyimide substrate with an appropriate herringbone pattern by means of atomic force microscope (AFM) scribing [4]. The pattern serves as an easy axis for liquid crystal alignment, in which the director follows the pattern closely except in regions of high curvature, where the slope of the scribing direction changes sign. In these regions the director is unable to follow the pattern due to elastic forces, and instead of an abrupt change in orientation, the director changes smoothly over a length scale $2L = 2K_{33}/W_{\varphi}$. Here L is known as the "extrapolation length" and W_{φ} is the "quadratic anchoring strength coefficient" associated with the ability of the substrate to orient the liquid crystal. On approaching the smectic-*A* phase from above, the divergence of K_{33} results in a diverging extrapolation length L, and thus in a uniformation of the director. Owing to our ability to impose a spatially sharp change in the easy axis, here we visualize and measure the extrapolation length and its temperature variation directly above T_{NA} and find that it is in good agreement with continuum theory. Then, on passing through the transition temperature, bend deformation must be completely expelled from the smectic-*A* phase, analogous to the Meissner effect in which magnetic field is expelled from a type-I superconductor [1]. In principle this would result in a single domain smectic-*A* phase in which the director lies along some appropriate average easy axis. We find this to be the case for herringbone patterns having a short wavelength P. However, we show that when the wavelength of the herringbone pattern is sufficiently large, there is a crossover to a multidomain texture with a weak wavelength threshold. Analogous behavior for very short wavelength patterns ($P \ll L$) has been observed in the nematic phase [5–8], although the behavior reported herein at the nematic–smectic-*A* transition is intimately associated with the diverging smectic correlation lengths in the nematic phase.

II. EXPERIMENT

A cell was constructed from two clean glass substrates: One substrate—the "master"—was prepared so as to promote planar orientation with spatially varying azimuthal easy axes by means of AFM nanopatterning, while the second "slave" substrate was prepared to promote planar degenerate alignment. The master was prepared thus: A glass substrate was spin-coated with the polyimide RN1175 (Nissan Chemical Industries) and baked at 200 °C for 1 h. Six squares of nominal dimensions 100×100 μm^2, each separated by approximately 30 μm from the adjacent square(s), were scribed with a herringbone pattern using the stylus (Nanodevices Tap300) of an atomic force microscope (Thermomicroscopes Explorer). In this scheme stripes of parallel grooves separated by 200 nm were oriented azimuthally at an angle $\gamma = +15°$ with respect to the y axis in one region of the herringbone and at $\gamma = -15°$ in the adjacent region. Figure 1 shows a schematic diagram of the writing pattern. Each scribed square differed from the others only by its spatial

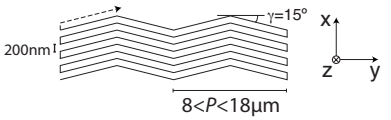

FIG. 1. Schematic of part of the herringbone pattern inscribed on the master substrate using the AFM stylus.

period P (along the y direction) of the stripes, viz., 8, 10, 12, 14, 16, and 18 μm. To prepare the slave surface, a clean glass substrate was spin-coated with warm (~40 °C) polymethylmethacrylate (PMMA) dissolved in 66 vol % propylene glycol methyletheracetate (PGMEA) with 33 vol % γ-butyrolacetone and baked at 80 °C for 2 h. The cell was assembled from the two substrates with mechanical clips. The thickness of the cell was measured to be 1.5 ± 0.1 μm using an interferometry technique. Finally, the cell was filled with the liquid crystal octyloxycyanobiphenyl ("8OCB," Merck) at temperature $T=76$ °C, i.e., in the nematic phase, and then slowly cooled. Experiments were performed above and below the nematic–smectic-A transition temperature $T_{NA}=67$ °C.

To observe the alignment of the liquid crystal in the patterned areas as a function of temperature, the cell was housed in an oven mounted on the stage of a polarizing microscope and viewed between crossed polarizers; all six squares were simultaneously within the field of view. A bandpass filter at wavelength 514.5 nm was inserted in the illumination light path to facilitate quantitative measurements over a narrow wavelength range. The cell was rotated so that the alignment direction of the herringbone lay at an angle of 22.5° with respect to the axis of one of the polarizers; this arrangement maximizes the contrast between the herringbone stripes of different orientation. The cell was cooled from the nematic phase and into the smectic phase at a rate of 20 mK min^{-1} and microscope images were taken at 2 mK intervals, i.e., once every 6 s.

Well above T_{NA} in the nematic phase, the herringbone pattern induced stripes at $\gamma=+15°$ and $-15°$ that appeared bright and dark, respectively [Fig. 2(a)], such that the intensity varied continuously in the region between adjacent stripes where the bend distortion is largest. Outside the well-aligned patterned regions, the nematic was found to exhibit a characteristic Schlieren texture. As the temperature was cooled to just above T_{NA}, the optical contrast between the stripes gradually diminished [Fig. 2(b)]. Figures 3(a) and 3(b) show regions of the herringbone patterns of periods 10 and 18 μm at a series of decreasing temperatures in the nematic phase. On cooling, it can be seen that the director associated with the shorter period patterns (8, 10, and 12 μm) becomes uniformized, culminating in a near uniform orientation along the y axis at the lowest temperature, which is 120 mK inside the smectic-A phase. This spatially uniform orientation can readily be seen: When the cell is rotated, the entire cell becomes nearly uniformly dark between crossed polarizers when the y axis is aligned with the polarizer. On the other hand, the integrity of the $\gamma=+15°$ and $-15°$ domains remains relatively unchanged on cooling into the smectic-A phase for the larger period herringbone, with a narrow domain wall in which the director varies continuously from one domain to the other. On cooling through the transition temperature T_{NA} into the smectic-A phase, the behavior in Fig. 2(c) was observed: Note that due to the bend distortion, the observed transition temperature is lowered slightly in the patterned regions relative to the unpatterned regions by $\sim l T_{NA} |\nabla \times \hat{\mathbf{n}}|$ [1] where l is the molecular length.

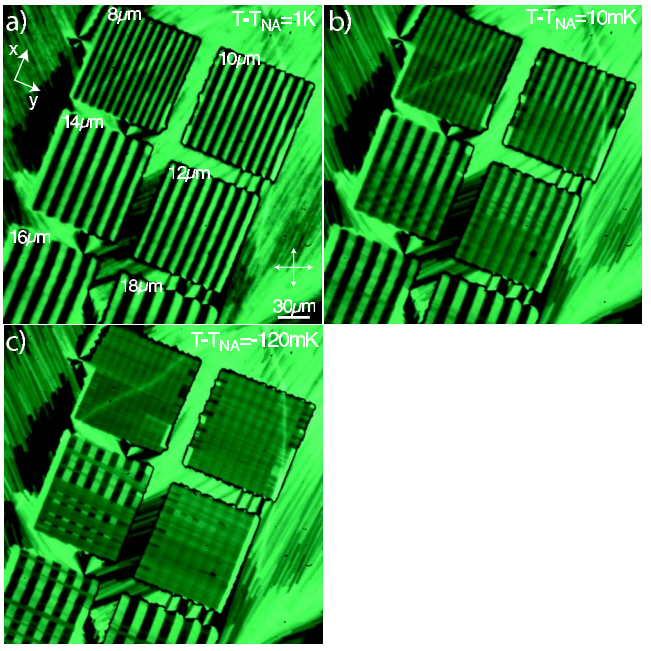

FIG. 2. (Color online) Polarizing microscope images of a cell with six herringbone patterns of indicated period at different temperatures: (a) nematic phase and (b) just above the N-A transition. (c) In the smectic phase. Notice uniform orientation on (c) for smaller period squares.

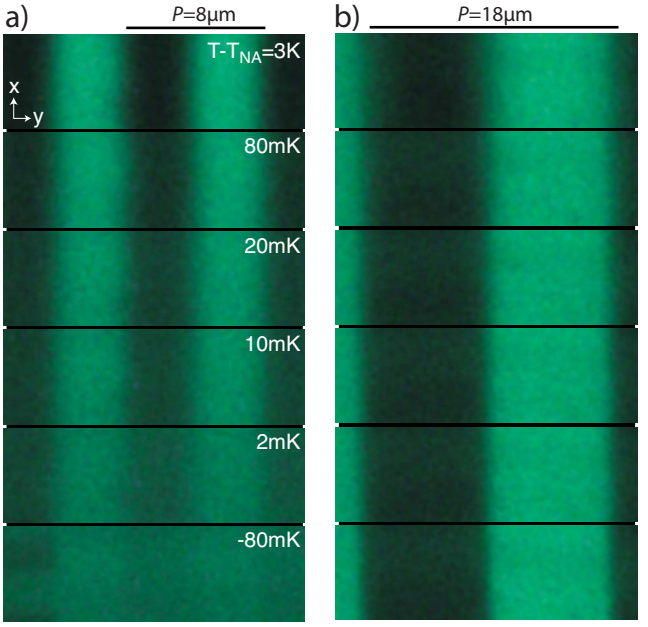

FIG. 3. (Color online) Detail of polarizing microscopy image at different temperatures showing (a) the uniformation process on a short-period pattern (and (b) division into domains of different orientation on a longer-period pattern.

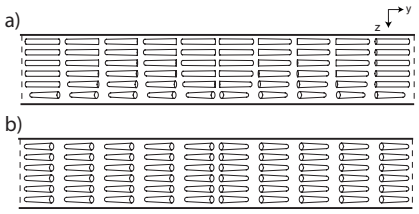

FIG. 4. Cartoons illustrating proposed director configurations at a temperature just above T_{NA} (a) uniformation and (b) division into domains separated by curvature walls.

The two configurations—a uniform director orientation associated with the shorter wavelength herringbones and a periodic director orientation associated with longer wavelength herringbones—are illustrated schematically in Figs. 4(a) and 4(b), where the view corresponds to that through the cell thickness. Both configurations are observed simultaneously for the two intermediate periods, namely of wavelength 14 and 16 μm, with roughly 50% and 10% of the patterned square covered by the uniform configuration, respectively. Each of these configurations remains stable upon further cooling through the smectic phase.

III. MODELING AND DISCUSSION

Let us now turn to a model for the observed behavior. In the nematic phase, just above T_{NA}, the Frank-Oseen nematic bulk free energy density f_b must be modified in the presence of smectic order fluctuations by including the temperature dependence of the twist and bend elastic constants

$$f_b = \frac{1}{2}K_{11}(\nabla \cdot \hat{\mathbf{n}})^2 + K_{22}(T)(\hat{\mathbf{n}} \cdot \nabla \times \hat{\mathbf{n}})^2 + K_{33}(T)|\hat{\mathbf{n}} \times \nabla \times \hat{\mathbf{n}}|^2, \tag{1}$$

where K_{11} is the splay elastic constant. The director configuration $\hat{\mathbf{n}}(r)$ adopted by the liquid crystal is that which minimizes the total energy. Extant theories for the variation of the elastic constants with temperature in the vicinity of the nematic–smectic-A phase transition assume the form [1,9]

$$K_{ii}(T) = K_{ii}^0 + \Delta K_{ii} t^{-\nu_i}, \quad i = 2,3, \tag{2}$$

in which the bare elastic constant K_{ii}^0 for the nematic phase is modified by a term that depends on the reduced temperature $t=(T-T_{NA})/T_{NA}$ with critical exponent ν_i.

In the present geometry, the herringbone pattern at the master surface tends to impose an elastic bend distortion on the bulk director. The extent to which the director follows the pattern in the region near the apexes is determined by competition between the elastic and anchoring strengths of the nematic: If the elastic constant of the dominant mode is large relative to the anchoring term, it is favorable for the director to rotate over a wider wall of width $2L$ at the expense of deviating from the easy axis imposed by the rubbing, and vice versa.

Away from the patterned surface, the elastic distortion relaxes toward a laterally uniform orientation in order to diminish the overall bend elastic energy; it must, however, do so at the expense of twist distortion. In the nematic phase of 8OCB, far above T_{NA}, the elastic constants satisfy the usual inequality for thermotropic nematics, $K_{22}<K_{11}<K_{33}$ [10] and are of approximate relative magnitude $K_{11}\approx 2K_{22} \approx 2/3K_{33}$ [10,11]. From the solution of Laplace's equation, the length scale in the z direction over which the director relaxes by twisting is $l_z \sim L\sqrt{K_{22}/K_{33}}<L$. Since $\nu_3>\nu_2$, K_{33} always is greater than K_{11} and K_{22}, and thus l_z decreases with decreasing temperature toward T_{NA}.

Although analytical solutions for $\hat{n}(r)$ may be obtained in some instances such as certain one-dimensional problems or where some of the elastic constants are equal [12], for the more complex geometry here it is necessary that the Euler-Lagrange equations be solved numerically. For our system the director is constrained at both surfaces to lie parallel to the substrate. The magnitude of any out-of-plane component of the director must therefore be small and so the director may be represented by a single (azimuthal) angle φ,

$$\hat{n}(y,z) = [\sin\varphi(y,z), \cos\varphi(y,z), 0], \tag{3}$$

the Euler-Lagrange equation obtained from Eq. (1) is

$$\mathcal{E}_\varphi = \frac{\partial f_b}{\partial \varphi} - \nabla \frac{\partial f_b}{\partial \nabla \varphi} = 0, \tag{4}$$

which may be discretized by cell-centered finite difference operators [13]

$$\nabla\varphi \to \left(\frac{\varphi_{i+1,j}-\varphi_{i-1,j}}{2\delta y}, \frac{\varphi_{i,j+1}-\varphi_{i,j+1}}{2\delta z}\right),$$

$$\nabla^2\varphi \to \frac{\varphi_{i+1,j}+\varphi_{i-1,j}-2\varphi_{i,j}}{\delta y^2} + \frac{\varphi_{i,j+1}+\varphi_{i,j-1}-2\varphi_{i,j}}{\delta z^2},$$

$$\frac{\partial^2\varphi}{\partial y\,\partial z} \to \frac{(\varphi_{i+1,j}-\varphi_{i-1,j})(\varphi_{i,j+1}-\varphi_{i,j-1})}{4\delta y\,\delta z}, \tag{5}$$

where the $\varphi(y,z)$ is represented on the vertices of a rectangular mesh $\varphi_{i,j}$ with a unit cell of size $\delta y \times \delta z$. Assuming a surface anchoring energy density of the Rapini-Papoular form [14],

$$f_s = \frac{1}{2}W_\varphi \sin^2[\varphi(y) - \varphi_e(y)], \tag{6}$$

where $\varphi_e(y)$ is the spatially dependent easy axis, the boundary condition may be derived from the balance of surface torques [12]

$$\hat{s}\frac{\partial f_b}{\partial \nabla \varphi} - \frac{\partial f_s}{\partial \varphi} = 0, \tag{7}$$

where $\hat{s}$ is the surface normal. Note that the surfacelike saddle-splay elastic term [15] with associated constant K_{24} does not enter the present analysis because deformations of the director field are constrained to a single plane. Derivatives with respect to the z coordinate in the boundary condition were discretized using asymmetric second-order finite difference operators of the type [13]

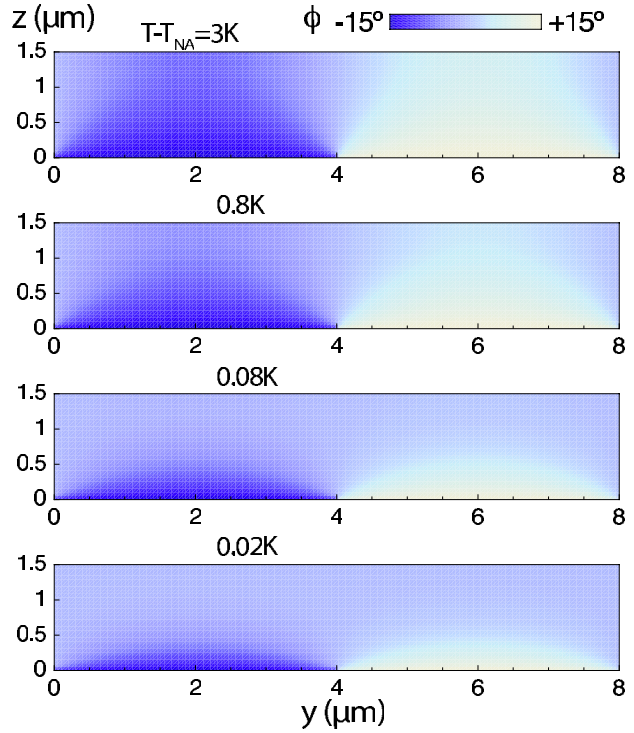

FIG. 5. (Color online) Simulated azimuthal director configurations for 8OCB in contact with a $P=8$ μm pattern at four temperatures above the nematic–smectic-A transition which occurs at $T=T_{NA}$.

$$\frac{\partial \varphi}{\partial z} \rightarrow \frac{3\varphi_{i,j} - 4\varphi_{i,j+1} + \varphi_{i,j+2}}{2\delta z}, \tag{8}$$

and periodic boundaries were imposed on the left- and right-hand sides. Free parameters for the system of Eqs. (4) and (7) are K_{11}, K_{22}, K_{33}, and P as well as boundary conditions $W_\varphi(y)$ and $\varphi_e(y)$; the solution $\varphi_{i,j}$ may then be obtained by taking successive Newton steps from an initial guess configuration until convergence. To ensure that the mesh has sufficient resolution to represent the solution, the solution was interpolated onto a finer mesh and the corresponding system of equations solved as before; this process of refinement was repeated until the solution converged.

The predicted configuration of the director as a function of temperature was calculated using the above procedure for each herringbone pattern. For each simulation at a particular temperature, numerical values of the ratios K_{11}/K_{33} and K_{22}/K_{33} were obtained from the parametrization due to Allender *et al.* [16] of Madhusudhana's measurements [10,11] of the elastic constants as a function of temperature. The anchoring strength coefficient W_φ and the elastic constant K_{11} were assumed to be independent of temperature over the small temperature range of the experiment. Calculated results for φ at several temperatures above T_{NA} are displayed in an edge-on view in Fig. 5. Consistent with the qualitative discussion above, the distorted bend region gradually becomes confined to the patterned surface as the bulk director becomes more spatially uniform with decreasing temperature in the nematic phase.

In order to facilitate comparison with experiment, we simulated the propagation of plane polarized light through the structure predicted from the continuum calculation. Numerical techniques such as finite difference time domain (FDTD) [17] have been used for this purpose but remain computationally expensive. A reasonable first-order approximation for normal incidence is to assume that the intensity of light observed at a single point under the polarizing microscope is due to a ray that has propagated as a plane wave and has passed through the liquid crystal immediately beneath the point of interest parallel to the z axis, remaining perpendicular to the substrates. In this way, the full two-dimensional optical calculation can be reduced to the parallel computation of many one-dimensional problems, since only the z variation of the director—and hence dielectric tensor—is incorporated into the calculation.

The optical calculation for intensity as a function of y proceeds as follows. The liquid crystal was divided into thin (≈ 1 nm) layers over which the director was treated as constant. Assuming a one-dimensional plane-wave solution, the electric and magnetic modes and associated eigenvectors were calculated for each layer using the Berreman 4×4 method [18]. The overall scattering matrix for the entire liquid crystal stack then was computed following Ref. [19] by matching the electric and magnetic fields at each layer interface. Propagating and evanescent modes were tracked separately to maintain numerical stability, and we verified that roundoff errors do not propagate by halving the size of the layers from 1 to 0.5 nm. The intensity transmitted following the analyzer was obtained from the appropriate element of the scattering matrix.

From images exhibiting the uniformation behavior, experimental intensity profiles as a function of y were obtained by averaging over a region 40 pixels (corresponding to about 6 μm) wide in the x direction. The calculated profiles were simultaneously fitted with two parameters (a multiplier and an offset) for all temperatures and herringbone spatial periods using a least-squares fit of the averaged profiles by way of the linear mapping $I_{\text{experimental}}=AI_{\text{calculated}}+B$, where A, B, and the transition temperature T_{NA} were treated as fitting parameters. A value $W_\varphi=0.2$ erg cm^{-2} [4] was used to calculate the director profiles, although the quality of fits as assessed from the residuals was found to be relatively insensitive to the anchoring strength coefficient beyond requiring the correct order of magnitude. A single value of T_{NA} was required for all fits but it was found necessary to allow A and B to vary weakly (to within 10%) among the different herringbone patterns; such a variation may be accounted for by nonuniformity of illumination and cell thickness. Representative fits at several temperatures are shown in Fig. 6. Despite the simplicity of the optical model, which does not account for diffraction limitations, the theoretical profiles are in excellent agreement with the images at the higher temperatures, although there is some small systematic deviation close to the transition. Such behavior is to be expected, as the modified nematic continuum theory used above holds only when the smectic correlation length is much less than the system size.

Let us now turn to the weak threshold behavior, whereby the liquid crystal becomes either uniformly oriented along

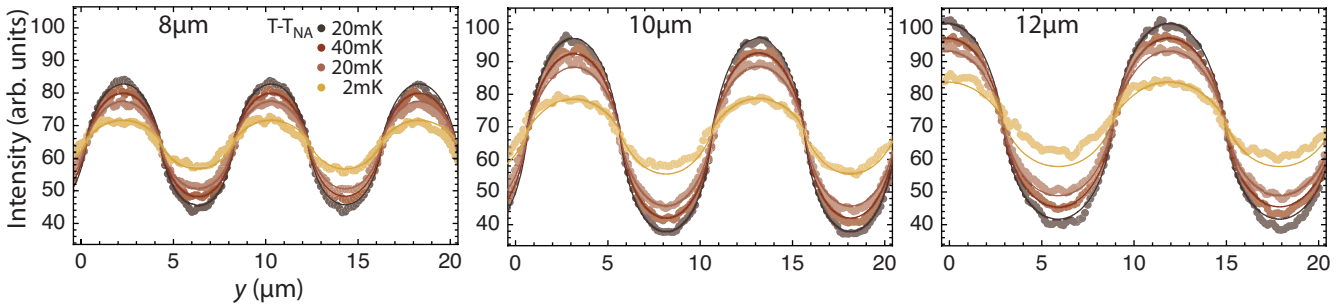

FIG. 6. (Color online) Representative fits of a simulated theoretical response from continuum theory and a simple optical model (solid lines) to intensity profiles obtained by averaging over multiple lines in the microscope images (circles). Herringbone periods are 8, 10, and 12 μm.

the y axis (for smaller P) or breaks into domains parallel to the local easy axes over most of the herringbone pattern (for larger P) as the temperature approaches T_{NA}. Although one might imagine that the divergence of the bend elastic modulus, and thus of the extrapolation length L, on approaching the transition temperature from above would result in a uniform director orientation at and below T_{NA}, this clearly is not the case for the patterns with larger periods. We speculate that when the correlation lengths $\xi_\perp$ and $\xi_\parallel$ become sufficiently large on cooling toward T_{NA} so as to be a significant fraction of the associated relaxation lengths l_z and L, the smectic order becomes "locked in" at this critical temperature T_c. (We note that K_{ii} diverges as Eq. (2) with a constant background term K_{ii}^0, whereas $\xi_{\perp,\parallel}$ has only a divergent part. Thus the correlation lengths can approach and crossover the relaxation lengths as $T \to T_{NA}$ from above.) If at this temperature the bend distortion occurs over a small length scale relative to half of the herringbone period P, i.e., $2L \ll P/2$, the smectic will break into domains, each of width $\sim P/2$. On the other hand, if $2L \gg P/2$ at T_c, then a spatially uniform smectic domain is more favorable. The actual crossover from one behavior to the other is complicated due to the presence of higher Fourier components associated with the herringbone pattern, surface memory effects involving an evolution of W_φ with time, and local defects that may serve as nucleation sites. In particular, the higher Fourier components likely will cause the actual crossover to occur when L is somewhat smaller than $P/4$. Now consider 8OCB at $T \sim T_{NA}+30$ mK, the temperature at which the two behaviors (uniform vs multiple domains) appear to begin their differentiation in Fig. 3. At this temperature, L becomes comparable to $P/4 \approx 3$ μm [20], the period experimentally associated with the crossover from multidomain (longer periods) to a uniform monodomain (shorter periods). As noted above, the presence of higher Fourier components in the distortion field likely drives the crossover to occur for values of L smaller than $P/4$. Given this and other spurious effects, the simple picture of monodomain vs polydomain behavior presented here must be considered only approximate.

IV. CONCLUSION

To summarize, we have imaged directly the growing extrapolation length L as the temperature of the liquid crystal is cooled toward the nematic–smectic-A phase transition. Based on continuum elastic theory and a simple optical model, calculations for the transmitted intensities were found to be in good agreement with the measured profile as a function of temperature. Additionally, we observed a soft threshold behavior on cooling toward T_{NA} when the liquid crystal is subjected to a bend distortion by herringbone nanopatterns of different spatial periods. For short periods the bend distortion is expelled completely, with the director field adopting a uniform bulk configuration. For long periods the smectic breaks into domains that are separated by curvature walls. On cooling toward T_{NA}, the observed behavior is consistent with the mechanism for which the director pattern (uniform or domain) becomes locked in at a critical temperature $T_c > T_{NA}$ at which the smectic correlation length grows to the same order as the associated relaxation lengths. If at this temperature the extrapolation length L is much smaller than half the herringbone period multiple domains obtain, in the opposite limit a monodomain appears.

Polarizing microscopy of the uniformation process yields an excellent signal-to-noise ratio and offers the intriguing possibility of probing the critical parameters of the nematic–smectic-A transition through machine vision techniques. Since such techniques are highly scalable, and require only sufficient material to cover the pattern, they are readily adaptable to high throughput methods. A more robust model to facilitate the solution of this inverse problem is presently under development.

ACKNOWLEDGMENTS

We thank Professor Rolfe G. Petschek for useful discussions. This work was supported by the Department of Energy's Office of Basic Energy Sciences under Grant No. DE-FG02-01ER45934 and by the National Science Foundation's Solid State Chemistry program under Grant No. DMR-0345109.

[1] P. G. de Gennes, Solid State Commun. **10**, 753 (1972).
[2] W. L. McMillan, Phys. Rev. A **4**, 1238 (1971).
[3] S. R. Renn and T. C. Lubensky, Phys. Rev. A **38**, 2132 (1988).
[4] R. Wang, I. M. Syed, G. Carbone, R. G. Petschek, and C. Rosenblatt, Phys. Rev. Lett. **97**, 167802 (2006).
[5] B. Zhang, F. K. Lee, O. K. C. Tsui, and P. Sheng, Phys. Rev. Lett. **91**, 215501 (2003).
[6] J. T. K. Wan, O. K. C. Tsui, H.-S. Kwok, and P. Sheng, Phys. Rev. E **72**, 021711 (2005).
[7] J.-H. Kim, M. Yoneya, and H. Yokoyama, Nature (London) **420**, 159 (2002).
[8] J.-H. Kim, M. Yoneya, and H. Yokoyama, Appl. Phys. Lett. **83**, 3602 (2003).
[9] S. Chandrasekhar, *Liquid Crystals*, 2nd ed. (Cambridge University Press, Cambridge, England, 1992).
[10] P. P. Karat and N. V. Madhusudhana, Mol. Cryst. Liq. Cryst. **40**, 239 (1977).
[11] N. V. Madhusudana and R. Pratibha, Mol. Cryst. Liq. Cryst. **89**, 249 (1982).
[12] I. W. Stewart, *The Static and Dynamic Continuum Theory of Liquid Crystals* (Taylor & Francis, London, 2004).
[13] W. H. Press, S. A. Teukolsky, W. T. Vetterling, and B. P. Flannery, *Numerical Recipes in C: The Art of Scientific Computing* (Cambridge University Press, Cambridge, England, 1988).
[14] A. Rapini and M. Papoular, J. Phys. Colloq. **30**, C4 (1969).
[15] G. P. Crawford and S. Zumer, Int. J. Mod. Phys. B **9**, 2469 (1995).
[16] D. Allender, R. Hornreich, and D. Johnson, Phys. Rev. Lett. **59**, 2654 (1987).
[17] E. E. Kriezis, C. J. P. Newton, T. P. Spiller, and S. J. Elston, Appl. Opt. **41**, 5346 (2002).
[18] D. W. Berreman, J. Opt. Soc. Am. **62**, 502 (1972).
[19] D. Y. K. Ko and J. R. Sambles, J. Opt. Soc. Am. A **11**, 1863 (1988).
[20] J. D. Litster, J. D. Als-Nielson, R. J. R. J. Birgeneau, S. S. Dana, D. Davidov, F. Garcia-Golding, M. Kaplan, C. R. C. R. Safinya, and R. Schaetzing, J. Phys. Colloq. **40**, C3 (1979).